Korean J. Chem. Eng., 40(6), 1510-1517 (2023)
DOI: 10.1007/s11814-023-1389-z

pISSN: 0256-1115
eISSN: 1975-7220

Preparation of carbonaceous monolith from polyacrylonitrile@lignin hybrid composite and its sensing and adsorption capability

Byung-Ho Kang*,‡, Jinyong Hong,‡, Oh-Nyoung Hur*, Minji Kang***, Jiyun Moon***, Jooyoung Seo***, Gyeongrim Han***, Suhyun Shin***, Chang-Soo Lee****,*****,†, Sung-Hoon Park*,†, and Joonwon Bae***,†**

*Department of Mechanical Engineering, Soongsil University, Seoul 06978, Korea
**Center for C1 Gas & Carbon Convergent Research, Korea Research Institute of Chemical Technology (KRICT), Yuseong-gu, Daejeon 34114, Korea
***Department of Applied Chemistry, Dongduk Women's University, Seoul 02748, Korea
****Bionanotechnology Research Center, Korea Research Institute of Bioscience & Biotechnology (KRIBB), Yuseong-gu, Daejeon 34141, Korea
*****Department of Biotechnology, University of Science & Technology (UST), Yuseong-gu, Daejeon 34113, Korea
(*Received 4 October 2022 • Revised 7 December 2022 • Accepted 26 December 2022*)

Abstract−A carbonaceous monolith material was produced from polyacrylonitrile@lignin (PAN@lig) composite hybrid; the sensing and adsorption capabilities of the material were evaluated. Because the two carbon-based precursors, PAN and lignin, have different characteristics, the resulting carbonaceous hybrid material was expected to exhibit unique properties. The controlled carbonization of PAN@lig produced a carbonaceous monolith with characteristic external and internal structures. Electron microscopy and cyclic voltammetry analyses of the morphological and electrochemical features of the monolith revealed stable structural and electrochemical properties. The hybrid, which acted as an electrochemical capacitor because of the electrical conductivity of the monolith, was suitable for use as a sensing material. The feasibility of using the carbonaceous monolith as a sensing medium was demonstrated by extensive electrical measurements of a simple sensor geometry. The carbonaceous hybrid also demonstrated the capacity to adsorb toxic chemicals/substances, such as radioactive heavy metal ions. The adsorption behavior was analyzed using several isotherm and kinetic models.

Keywords: Adsorption, Carbonaceous Monolith, Lignin, Polyacrylonitrile, Sensor

INTRODUCTION

The use of naturally abundant and nontoxic materials is important for environmental conservation and economics. Among these materials, wood and plant components (e.g., cellulose and lignin) have received considerable attention because of their prevalence and abundance [1-3]. Cellulose is particularly useful for paper production, filtration, and packaging [4]. Lignin, which is obtained in large quantities as a major byproduct of paper production, is attractive because it and its derivatives have intriguing properties that include mechanical durability, chemical resistance, and high adsorption capacity [5-10]. Although it is challenging to fractionate lignin into valuable monomeric substances, there is increasing interest in exploring the utility of lignin [11-13].

The carbonization of cellulose and lignin generates unique types of carbonaceous materials [2,5,6,14]. For example, the carbonization of lignin can produce carbonaceous materials with highly cross-linked and networked structures because lignin is predominantly composed of phenolic groups [15]. The resulting structures are analogous to the structures of semicrystalline carbonaceous materials derived from polymeric precursors with generally high crystallinity [16]. Additionally, carbonized lignin products are expected to exhibit excellent adsorption capacity because of inherent micropores [9, 10,17,18]. A controlled carbonization profile is essential for the maintenance of a porous structure during thermal treatment [19]. Carbonized lignin products may be suitable for diverse applications, such as adsorbents, water treatment, and toxic gas removal [20]. Nevertheless, carbonized lignin generally has a loose structure with low surface area [15].

The incorporation of additional materials is one of the best strategies to further improve the performance of carbonized products derived from lignin [21-24]. Lignin can be modified to improve its compatibility with various organic, polymeric, and inorganic materials [25,26]. In terms of manufacturing and processing applications, the addition of polymeric carbon precursors as compatibilizers is a preferred approach. Among these precursors, polyacrylonitrile (PAN) is noteworthy [27,28]. Its advantages include favorable interactions with phenolic groups, a stable structural transition during the carbonization step, and high structural regularity [29]. Additionally, strong favorable interactions between CN and phenol groups can sustain structural robustness during the mixing and carbonization processes. Thus, the carbonization of a PAN@lig precursor can com-

†To whom correspondence should be addressed.
E-mail: cslee@kribb.re.kr, leopark@ssu.ac.kr, redsox7@dongduk.ac.kr, joonwonbae@gmail.com
‡These authors equally contributed to this work.

pensate for the heterogeneity of the precursor components and yield unique carbonaceous materials [30-32]. The practical applications of carbonized products from a PAN@lig precursor, which are typically in the form of nanofibers [33-36], include secondary battery anodes, supercapacitors, and electromagnetic shielding.

In this work, a carbon monolith film was derived from a PAN@lig precursor film through a controlled carbonization profile that consisted of stabilization at a low heating rate, carbonization at a medium heating rate, holding at a maximum temperature, and unforced cooling. The possibility of using the controlled cycle for carbonization of a lignin precursor was investigated. The morphology and surface property of the carbonized monolith were examined before and after carbonization. The electrical conductivity was measured, and the electrochemical properties were investigated using cyclic voltammetry (CV). The carbon monolith was evaluated as a sensing medium for the detection of chemicals (NH_3) using various electrical measurement techniques. Additionally, its adsorption capacity and behavior toward chemicals of medium polarity (e.g., methyl paraben) and heavy metal ions (e.g., Cs^+) were analyzed.

EXPERIMENTAL

1. Materials

Polyacrylonitrile (average molecular weight: 150,000 g mol^{-1}); lignin; N, N-dimethylformamide (purity >99.8%); and methyl paraben were purchased from Sigma-Aldrich Chemical Co. (Milwaukee, WI, USA) and used as received. Ethanol was purchased from Samchun Chemical Co. (Seoul, Republic of Korea).

2. Preparation of PAN@Lig Films

Polyacrylonitrile (1 g) was dissolved in N, N-dimethylformamide (10 mL). The solution was sonicated for 1 h and stirred vigorously overnight at room temperature. Lignin powder was added to the solution at 7.5, 15, or 25 wt% with respect to PAN; the resulting mixture was agitated using a homogenizer for 30 min. The solution was then cast on a glass substrate and the film was prepared using a doctor blade. Then, the film was dried overnight at 80 °C and additionally under vacuum for 3 h. The thickness of the prepared film was approximately 200 μm.

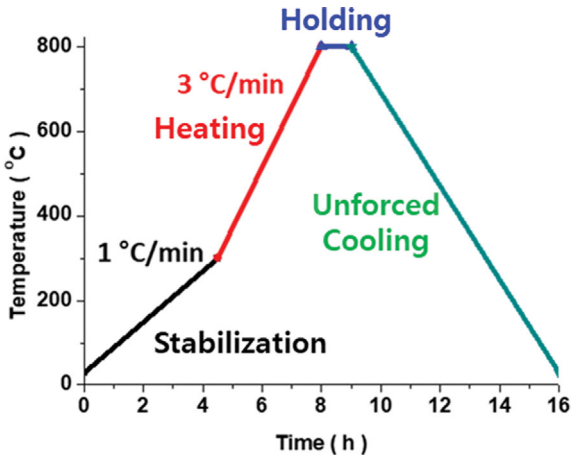

Fig. 1. A carbonization cycle with a temperature profile used for PAN@Lig precursors.

3. Carbonization of PAN@Lig Films

A controlled carbonization cycle was adopted for effective conversion of the PAN@lig precursor to carbonaceous materials. The carbonization process consisted of four major steps: stabilization (1 °C min^{-1} to 300 °C), heating (3 °C min^{-1} to 800 °C), holding (1 h), and unforced cooling (Fig. 1). This cycle helped to improve conversion efficiency and structural uniformity [15,19].

4. Adsorption Tests

A solution of methyl paraben in ethanol (10^{-4} M) was prepared and separated into several vials. Carbonized PAN@lig film (0.05 g) was added to each of the vials containing the methyl paraben solution. An aliquot was removed from each vial and the UV absorbance was measured. The same experiment was conducted with the carbonized PAN film.

Stable $^{133}Cs^+$ ion was used, rather than radioactive $^{137}Cs^+$. A solution containing $^{133}Cs^+$ ion was prepared by adding the $^{133}Cs^+$ standard solution (1 ppm) containing 60% HNO_3 to distilled water (100 mL). Then, a defined amount of adsorbent was added to the resulting solution and the mixture was shaken at 300 rpm. The adsorption capacity was monitored from 0 to 6 h. After the adsorption process, the solution was filtered through a syringe (PTFE-H; pore size: 0.2 μm; Hyundai Micro), and the ion concentration was determined by elemental analysis.

5. Instrumentation

Fourier transform-infrared and ultraviolet-visible (UV-vis) spectra were obtained using Perkin Elmer Spectrum One (Perkin Elmer, USA) and UV1200 (Shimadzu, Japan) spectrometers, respectively. Morphological features were observed using a scanning electron microscope (JEOL 6700; JEOL, Japan) with an accelerating voltage of 10 kV. Electrical conductivity was measured using the standard four-probe method. Electrochemical properties were examined by CV at a sweep rate of 100 mV s^{-1} using a potentiostat (PalmSens4; PalmSens, Netherlands) equipped with a conventional three-electrode beaker-type cell that contained 1 M H_2SO_4 as the electrolyte. A 6-cm-long platinum wire and Ag/AgCl served as the counter and reference electrodes, respectively. Sensing performance was evaluated by electrical measurements using a source meter (Keithley 2612 B; Tektronix, USA) equipped with a probe (MST 4000A; MSTECH, Korea). The device architecture is schematically illustrated in Fig. 2. A typical polar molecule, NH_3 was introduced as analyte in ethanol. Changes in the electrical current were normal-

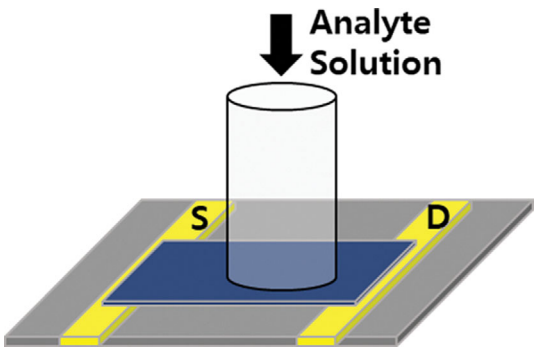

Fig. 2. Schematic illustration of sensor geometry using carbonized PAN@lig film.

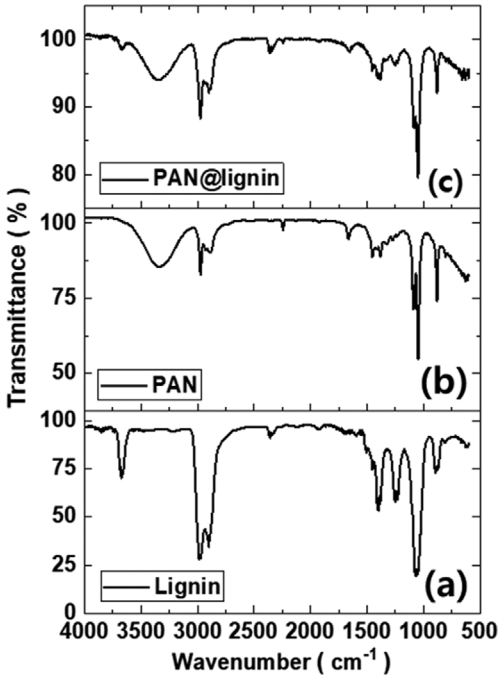

Fig. 3. Fourier transform-infrared spectra of (a) lignin, (b) PAN, and (c) PAN@lig (15 wt%) precursor film.

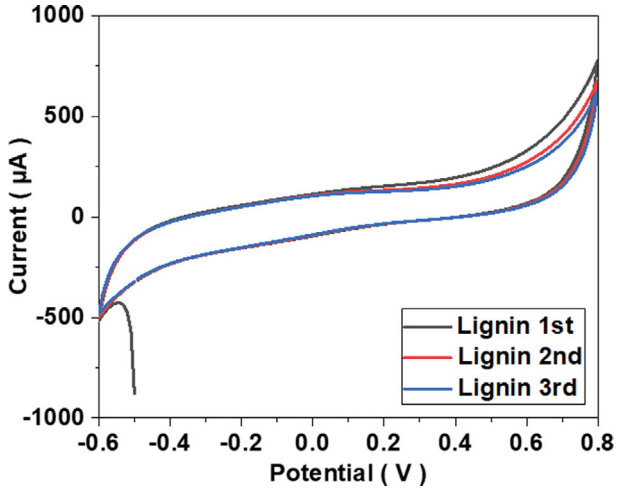

Fig. 4. Cyclic voltammetry profiles of lignin obtained in 1 M H_2SO_4 at a scan rate of 100 mV/s.

ized according to $\Delta I/I_0=(I-I_0)/I_0$, where I_0 and I are the initial and detected currents, respectively. Inductively coupled plasma-mass spectrometry (iCAP RQ; Thermo Fisher Scientific, USA) was used to determine the concentration of $^{133}Cs^+$ ion in solution.

RESULTS AND DISCUSSION

The first requirement for production of the carbonized PAN@lig was the preparation of a uniform PAN/lignin mixture that would ultimately be used to produce the PAN@lig precursor film. The formation of a homogeneous PAN@lig precursor film was confirmed using Fourier transform-infrared spectroscopy. Strong peaks at approximately 3,000 and 3,300 cm^{-1} were attributed to C-H and phenolic O-H stretching vibrations, respectively (Fig. 3(a)). A strong peak at approximately 1,100 cm^{-1} was attributed to the bending of C-H bonds in benzene rings. A medium-intensity band at 1,300 cm^{-1} was attributed to C=O linkages in phenol structures. A sharp peak of low intensity at approximately 2,200 cm^{-1} was attributed to the C≡N groups in PAN (Fig. 3(b)). All characteristic peaks of both PAN and lignin were observed in the Fourier transform-infrared spectrum of the PAN@lig precursor film (Fig. 3(c)).

This study explored the sensing and adsorption behaviors of carbonized PAN@lig monolith film. Thus, the basic properties of the components were examined. Although the fundamental properties of PAN polymer have been extensively studied [37], the properties of lignin have received less attention. Fig. 4 shows the CV profiles of lignin; no oxidation/reduction reactions are apparent. These findings indicated that the functional groups on the surface of lignin were stable and supported the hypothesis that lignin functions as an adsorbent without initiating reactions during adsorption uptake. The mechanism of lignin carbonization might be analogous to the mechanism of carbonization involving phenolic polymer precursors because the chemical structures of lignin and phenolic polymers are similar, and surface reactions must be minimal during lignin carbonization. Notably, lignin exhibited a limited capacity for charge storage because the CV profiles had a parallelogram shape. This means that the charge is accumulated in the inner surface, even after carbonization. This finding also implies that the carbonized product possesses a certain amount of surface area, which is critical for sensing and removal of toxic substances.

Carbonization of the PAN@lig precursor film was expected to be substantial because the two precursors are readily carbonized. However, PAN and lignin have different thermal expansion coefficients, which could induce stress at the PAN-lignin interface, disrupt the internal carbonaceous structure, and cause performance deterioration. The observation of irregular macropores in the fracture surface would serve as evidence of this phenomenon. Accordingly, the morphological features of the carbonized products were examined using a scanning electron microscope (Fig. 5). For the PAN film, the morphological characteristics remained almost intact after carbonization (Fig. 5(a) and 5(b)). In contrast, the PAN@lig film exhibited some notable features (Fig. 5(c)-5(f)). A few raised structures, clearly evident on the top surface of the carbonized PAN@lig monolith film, were attributed to the incorporated lignin (Fig. 5(d)); the PAN@lig precursor film did not exhibit these features (Fig. 5(c)). This pattern was also observed for the PAN@lig precursor film that showed high lignin loading (Fig. 6). No macropores were evident on the fracture surface of the carbonized PAN@lig monolith film (Fig. 5(f)), which indicated that the resulting carbonaceous structure was robust and stable. Although the PAN/lignin-derived carbonaceous structures presumably differed at the atomic level, such heterogeneity could be useful for certain applications.

Similar morphological features were observed when the lignin content of the PAN@lig film was high (i.e., 25 wt%) (Fig. 6). Raised structures were observed because of the added lignin (Fig. 6(a)), and some mesopores were observed after carbonization (Fig. 6(b)). However, the pores did not affect the stability or robustness of the three-dimensional structure. Additionally, lignin-derived carbon

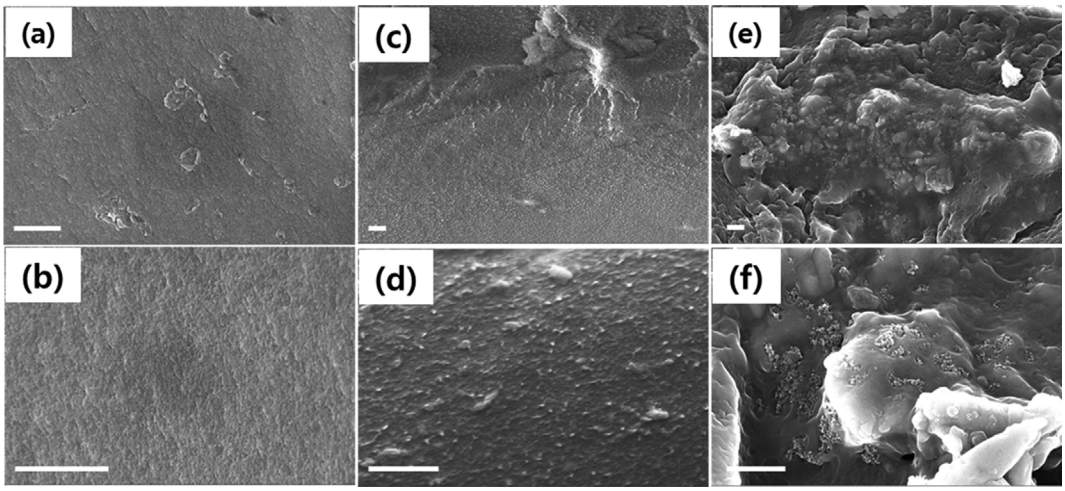

Fig. 5. Scanning electron microscope images of the fracture surface of the PAN film (a) before and (b) after carbonization. Top and fracture surfaces of the PAN@lig (15 wt%) film (c), (e) before and (d), (f) after carbonization (scale bar: 1 μm).

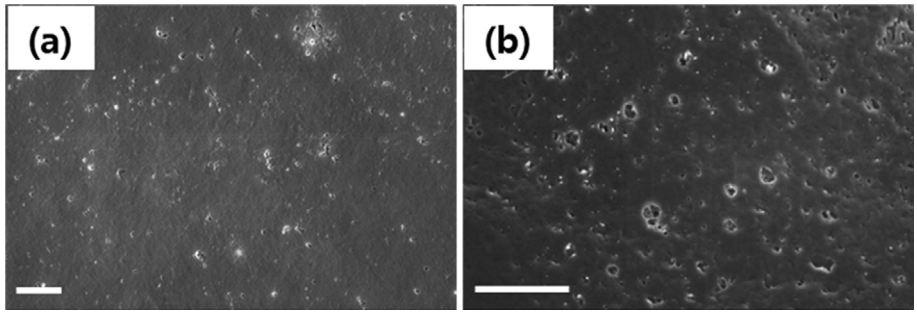

Fig. 6. Scanning electron microscope images of the fracture surface of the PAN@lig (25 wt%) film (a) before and (b) after carbonization (scale bar: 1 μm).

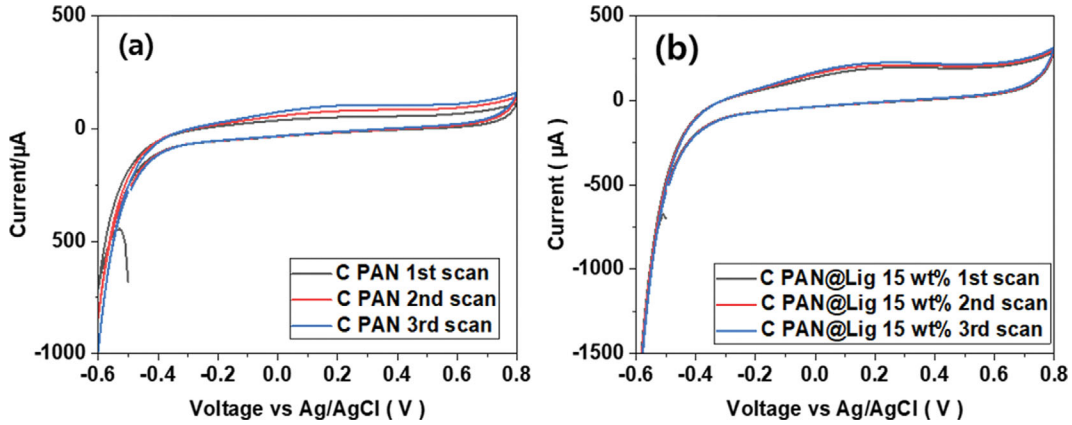

Fig. 7. Cyclic voltammetry profiles of carbonized (a) PAN and (b) PAN@lig films obtained in 1 M H_2SO_4 at a scan rate of 100 mV s^{-1}.

may be more polar than PAN-derived carbon, which could be a useful feature for sensing and adsorption applications.

The electrochemical properties of the carbonized PAN and PAN@lig films were examined for comparison of their sensing and adsorption behaviors. The CV profiles confirmed that no oxidation/reduction reactions occurred (Fig. 7); the tetragonal shape indicated that the carbonized films exhibited weak charge storage capacity, presumably related to the presence of generated pores and an increased surface area. The slightly larger area of the CV profile of carbonized PAN@lig (compared with the CV profile of carbonized PAN) was thus attributed to lignin addition. Accordingly, we anticipated that the carbonized PAN@lig monolith film would exhibit better sensing performance, compared with the carbonized PAN film.

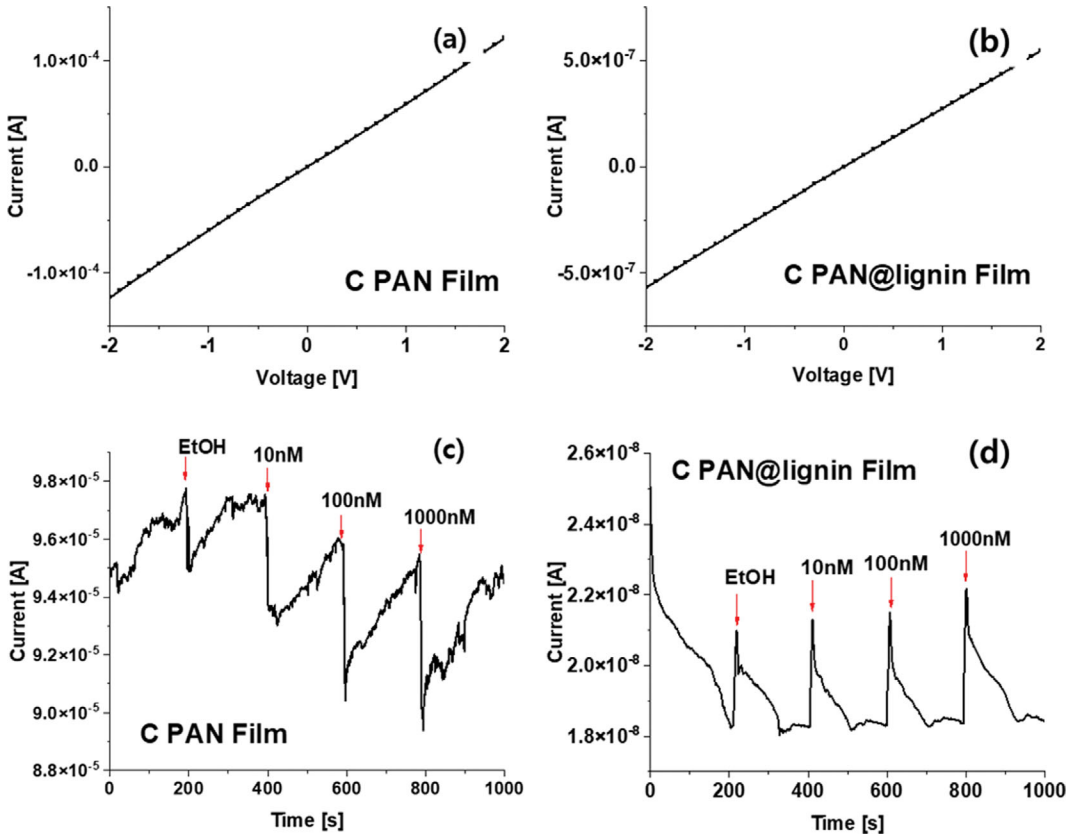

Fig. 8. Current-voltage curves showing ohmic relationships for the carbonized (a) PAN and (b) PAN@lig films. Electrical sensing signal profiles of the carbonized (c) PAN and (d) PAN@lig for ethanolic NH_3 solutions.

A simple device was fabricated to investigate the possibility of using the carbonized PAN@lig monolith film as a sensing medium (Fig. 2). Because the sensing signal was transported through the carbonized film body, the electrical conductivity of the film was important. The electrical conductivity of the carbonized PAN@lig film (approximately 10^{-4} S cm^{-1}) was slightly lower than the electrical conductivity of the carbonized PAN film because of the insulating nature of lignin. This suggested that the electrical conductivity would respond to the addition of analyte substances; the resulting electrical signal would thus be proportional to the concentration of the analyte. To obtain reliable sensing signal profiles, simple voltage sweep tests were conducted with the carbonized PAN and PAN@lig films to confirm stable ohmic relationships (Fig. 8(a) and 8(b)). Solvent addition tests were also performed to exclude the solvent effect on electrical signals because analyte samples were introduced in solution for the liquid-state sensor used in this work; the effect of EtOH solvent was minimal (Fig. 8(c) and 8(d)) [15]. The sensing profiles as a function of analyte concentration were obtained with successive addition of analyte solution. The signal intensity was proportional to the concentration; this finding indicated that charge transport between the analyte and sensing medium was facilitated at higher concentrations. Notably, the profile of the carbonized PAN@lig film was less noisy than the profile of the carbonized PAN film. Furthermore, the current change observed for the carbonized PAN@lig film was much smaller than the current change observed for the carbonized PAN film. This behavior was caused by the lower electrical conductivity of the carbonized PAN@lig film, compared with the carbonized PAN film, as noted above.

The adsorbent properties of lignin have been extensively characterized. Two types of analytes—polar methyl paraben and $^{133}Cs^{+}$ metal ion—were selected for adsorption studies. Fig. 9 presents the UV-vis spectra obtained as a function of adsorption time after immersion of the carbonized PAN (Fig. 9(a)) and PAN@lig (Fig. 9(b)) films in 10^{-4} M methyl paraben solution. The observed negligible adsorption of methyl paraben molecules by the carbonized PAN and PAN@lig films was associated with the unfavorable interaction between apolar carbonized products and polar methyl paraben molecules. The UV-Vis spectra in Fig. 9(b) show that the adsorption of paraben molecule was insignificant, even if carbonized lignin was used with carbonized PAN. This means that the effect of carbonized lignin on adsorption was also insignificant.

We anticipated that the pristine PAN@lig film would exhibit a different adsorption pattern toward heavy metal ions because of the excellent adsorption capacity of lignin [15]. To examine the adsorption behavior and mechanism, several tests were conducted as a function of contact time at 20 °C and pH 7.0. The $^{133}Cs^{+}$ ion uptake was calculated according to the following equation:

$$q_e = \frac{(C_o - C_e)V}{W} \quad (1)$$

where q_e is the equilibrium adsorption capacity of the adsorbent (mg g^{-1}), C_o is the initial ion concentration (mg L^{-1}), C_e is the equi-

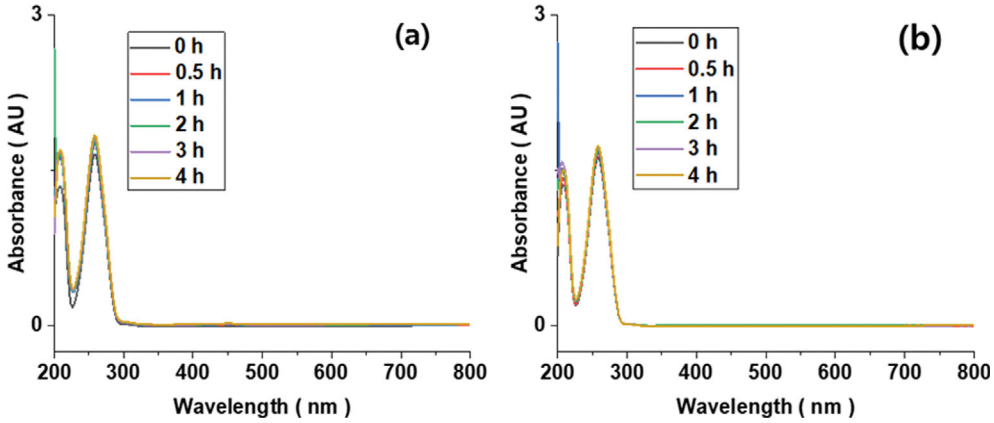

Fig. 9. UV-vis spectra of the carbonized (a) PAN and (b) PAN@lig films after immersion for various times in 10^{-4} M methyl paraben solution.

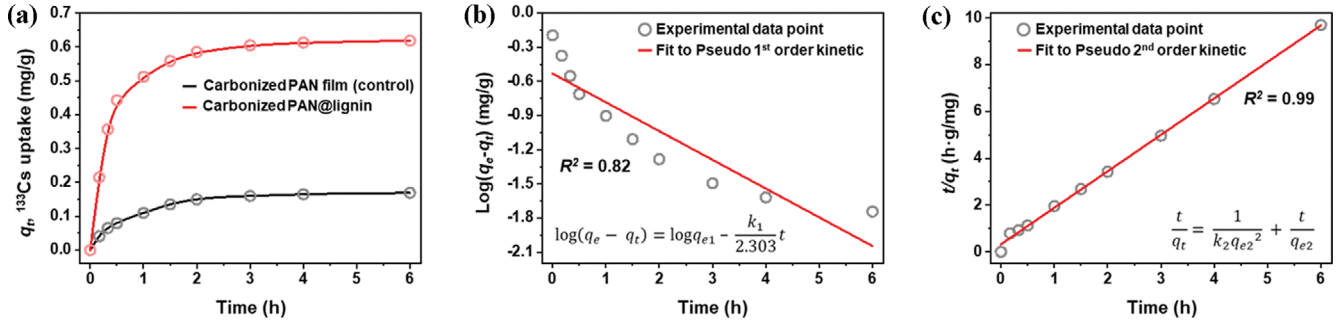

Fig. 10. (a) $^{133}Cs^+$ ion uptake behavior as a function of contact time and adsorption isotherms for $^{133}Cs^+$ ion uptake for the carbonized PAN@lig film fitted to (b) pseudo-first-order and (c) pseudo-second-order kinetic models (initial concentration: 1.0 ppm; adsorbent dosage: 1.0 g L^{-1}; pH: 7.0; temperature: 20 °C).

Table 1. Adsorption parameters of the pseudo-first-order and pseudo-second-order kinetic models at room temperature for the adsorption of $^{133}Cs^+$ ion on the carbonized PAN@lig film

	Pseudo-first-order[a]			Pseudo-second-order[a]		
	k_1 (1/h)	q_{e1} (mg/g)	R^2 [b]	k_2 (1/h)	q_{e2} (mg/g)	R^2 [b]
^{133}Cs	0.58	0.29	0.82	7.46	0.64	0.99

[a]The k_1, q_{e1}, k_2 and q_{e2} values were measured by nonlinear regression analysis using OriginPro 8.5.
[b]R^2=determination coefficient.

librium ion concentration after adsorption (mg L^{-1}), V is the total volume of the solution (L), and W is the weight of the PAN@lig (g).

Fig. 10 presents the heavy metal ion uptake by the carbonized PAN@lig monolith film as a function of contact time; uptake reached saturation at 6 h. To explain the adsorption kinetics, the experimental results were fitted to pseudo-first-order (Fig. 10(b)) and second-order (Fig. 10(c)) kinetic models [38,39]. In the pseudo-first-order equation, q_e and q_t are the ion uptakes at equilibrium and at time t, respectively; k_1 is the rate constant of first-order adsorption (h^{-1}). In the pseudo-second-order equation, k_2 is the rate constant of second-order adsorption (g mg^{-1} h^{-1}). The adsorption behavior was best explained by the pseudo-second-order model, and the capacity of the carbonized PAN@lig film toward $^{133}Cs^+$ was better than the corresponding capacity of carbonized PAN film. However, the adsorption capacity was inferior to the reported capacity of a polypyrrole@lignin composite because the favorable chemical interaction between carbonized PAN@lig film and $^{133}Cs^+$ ion was weak compared with the interaction in the polypyrrole@lignin material [15]. Table 1 provides the adsorption parameters associated with the pseudo-first-order and pseudo-second-order kinetic models.

Equilibrium adsorption data were fitted to the Langmuir and Freundlich isotherm equations to better understand the adsorption process. Fig. 11 presents the ion uptake by the carbonized PAN@lig film as a function of equilibrium $^{133}Cs^+$ ion concentration at 20 °C and pH 7.0. The adsorption capacity was measured at 12 h of contact time (i.e., when adsorption equilibrium was achieved). The nonlinear plots obtained by fitting the experimental data to the Langmuir and Freundlich isotherms are presented in Fig. 11; the parameters and R^2 values for each model are listed in Table 2. The Freundlich model better explained the adsorption behavior of the

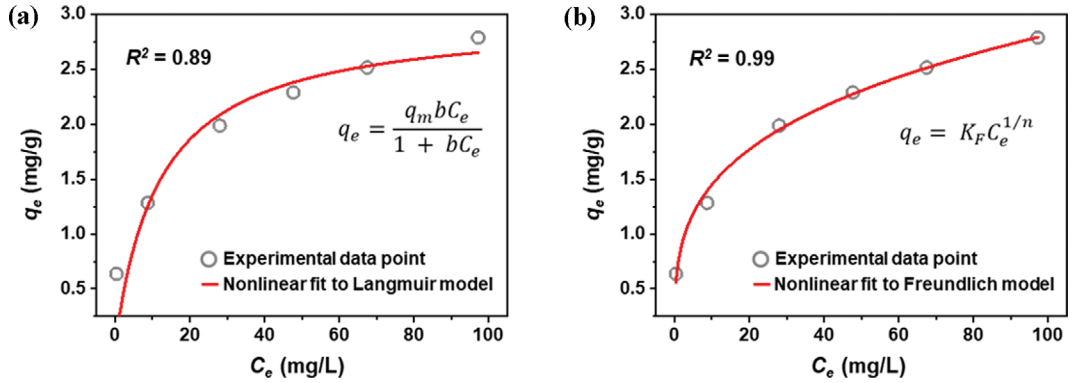

Fig. 11. $^{133}Cs^+$ ion uptake behavior as a function of equilibrium ion concentration and adsorption isotherms for $^{133}Cs^+$ ion uptake by the carbonized PAN@lig film. Nonlinear fitting of the data to the (a) Langmuir and (b) Freundlich isotherm equations (contact time: 12 h; pH: 7.0; temperature: 20 °C).

Table 2. Adsorption parameters of the Langmuir and Freundlich isotherm models at room temperature for the adsorption of $^{133}Cs^+$ ion on the carbonized PAN@lig film

	Langmuir[a]			Freundlich[a]		
	q_m (mg/g)	b (L/mg)	R^{2b}	K_F (mg/g)(L/mg)$^{1/n}$	n	R^2
^{133}Cs	2.98	0.08	0.89	0.75	3.47	0.99

[a]The q_m, b, K_F and n values were measured by nonlinear regression analysis using OriginPro 8.5.
[b]R^2=determination coefficient.

carbonized PAN@lig film, which implied that this film exhibited a heterogeneous surface for adsorption with abundant active sites.

CONCLUSIONS

A carbonized PAN@lig monolith film was prepared by controlled carbonization of PAN@lig precursor; the morphology and properties of the monolith film were characterized. The carbonized PAN@lig is a new carbonaceous material with significant electrical conductivity. The carbon film constitutes a robust and rigid sensor substrate for the detection and removal of potentially hazardous substances. Although the film shows a weak ability to remove organic molecules, it is useful for the uptake of heavy metal ions because of the affinity that lignin exhibits toward ionic species. The adsorption behavior was quantitatively examined and compared with the behavior of carbonized PAN film. This study provides important insights for future research activities in relevant fields, such as novel lignin-derived carbonaceous materials.

ACKNOWLEDGEMENTS

This research was supported by Korea Institute of Planning and Evaluation for Technology in Food, Agriculture and Forestry (IPET) and Korea Smart Farm R&D Foundation (KosFarm) through Smart Farm Innovation Technology Development Program, funded by Ministry of Agriculture, Food and Rural Affairs (MAFRA) and Ministry of Science and ICT (MSIT), Rural Development Administration (RDA) (421042-04). This work was also supported the Industrial Strategic Technology Development Program (20012763) funded by the Ministry of Trade, Industry & Energy (MOTIE, Korea) and by the National Research Foundation of Korea (NRF) grant funded by the Korea government (MSIT No. 2020R1A2C1013489 & NRF-2021R1F1A1061939).

DECLARATION OF COMPETING INTERESTS

There are no conflicts of interest or patent pending.

AUTHORS' CONTRIBUTIONS

Byung-Ho Kang: Data curation, Investigation, Methodology, Visualization, Writing - review & editing **Jin-Yong Hong**: Data curation, Investigation, Methodology, Writing - review & editing **Oh-Nyoung Hu**: Data curation, Investigation, Methodology **Minji Kang**: Data curation, Investigation, Methodology **Jiyun Moon**: Data curation, Investigation, Methodology **Jooyoung Seo**: Data curation, Investigation, Methodology **Gyeongrim Han**: Data curation, Investigation, Methodology **Suhyun Shin**: Data curation, Investigation, Methodology **Chang-Soo Lee**: Conceptualization, Funding acquisition, Investigation, Project administration, Supervision **Sung-Hoon Park**: Conceptualization, Funding acquisition, Investigation, Project administration, Supervision, Writing - original draft **Joonwon Bae**: Conceptualization, Funding acquisition, Investigation, Project administration, Supervision, Writing - original draft.

REFERENCES

1. Z. Jiadeng, Y. Chaoyi, Z. Xin, Y. Chen, J. Mengjin and Z. Xiangwu, *Prog. Energy Combust. Sci.*, **76**, 100788 (2020).
2. E. Svinterikos, I. Zuburtikudis and M. Al-Marzouqi, *ACS Sustain-*

able Chem. Eng., **8**, 13868 (2020).
3. E. Frank, L. M. Steudle, D. Ingildeev, J. M. Spörl and M. R. Buchmeiser, *Angew. Chem. Int. Ed.*, **53**, 5262 (2014).
4. L. Zhu and Z. Zhong, *Korean J. Chem. Eng.*, **37**, 1660 (2020).
5. A. A. Ahmad, M. Al-Raggad and N. Shareef, *Carbon Lett.*, **31**, 957 (2021).
6. Q. Yan, J. Li and Z. Cai, *Carbon Lett.*, **31**, 941 (2021).
7. P. K. Dikshit, H. B. Jun and B. S. Kim, *Korean J. Chem. Eng.*, **37**, 387 (2020).
8. S. Wang, L. Lyu, G. Sima, Y. Cui, B. Li, X. Zhang and L. Gan, *Korean J. Chem. Eng.*, **36**, 1042 (2019).
9. F. Flores-Céspedes, M. Villafranca-Sánchez and M. Fernández-Pérez, *Int. J. Biol. Macromol.*, **153**, 883 (2020).
10. J. Yang, J. J. Pignatello, B. Pan and B. Xing, *Environ. Sci. Technol.*, **51**, 8972 (2017).
11. X. Zhuang, M. C. Shin, B. J. Jeong, J. Y. Hwang, Y. C. Choi and J. H. Park, *Korean J. Chem. Eng.*, **39**, 1588 (2022).
12. Y. K. Lee, S. C. Chung, S. Y. Hwang, S. H. Lee, K. S. Eom, S. B. Hong, G. G. Park, B. J. Kim, J. J. Lee and H. I. Joh, *Korean J. Chem. Eng.*, **36**, 1543 (2019).
13. J. Behin, L. Rajabi, H. Etesami and S. Nikafshar, *Korean J. Chem. Eng.*, **35**, 602 (2018).
14. A. El Nemr, R. M. Aboughaly, A. El Sikaily, M. S. Masoud, M. S. Ramadan and S. Ragab, *Carbon Lett.*, **32**, 229 (2022).
15. O.-N. Hur, S. Park, S. Park, B.-H. Kang, C.-S. Lee, J.-Y. Hong, S.-H. Park and J. Bae, *Mater. Chem. Phys.*, **285**, 126166 (2022).
16. W. Thongpat, J. Taweekun and K. Maliwan, *Carbon Lett.*, **31**, 1079 (2021).
17. Y. Liu, X. Cheng and S. Zhang, *Carbon Lett.*, **32**, 251 (2022).
18. M. Vinayagam, R. S. Babu, A. Sivasamy and A. L. Ferreira de Barros, *Carbon Lett.*, **31**, 1133 (2021).
19. S. Joo, B. Kim, J. An, M. Park, S. Seo, J. Y. Park and J. Bae, *J. Mater. Sci.*, **53**, 9316 (2018).
20. A. F. Zakaria, S. Kamaruzaman and N. A. Rahman, *Polymers*, **13**, 3590 (2021).
21. Y. Guo, C. Cheng, T. Huo, Y. Ren and X. Liu, *Polym. Degrad. Stab.*, **181**, 109362 (2020).
22. Q. He, P. Zhou, J. Hao, C. Lu and Y. Liu, *ACS Omega*, **4**, 11346 (2019).
23. H. Clive Liu, C.-C. Tuan, A. A. Bakhtiary Davijani, P.-H. Wang, H. Chang, C.-P. Wong and S. Kumar, *Polymer*, **111**, 177 (2017).
24. H. Clive Liu, A.-T. Chien, B. A. Newcomb, A. A. Bakhtiary Davijani and S. Kumar, *Carbon*, **101**, 382 (2016).
25. Z. Dai, P.-G. Ren, Y.-L. Jin, H. Zhang, F. Ren and Q. Zhang, *J. Power Sources*, **437**, 22693 (2019).
26. S. Demiroğlu Mustafov, A. K. Mohanty, M. Misra and M. Özgür Seydibeyoğlu, *Carbon*, **147**, 262 (2019).
27. S. Li, W. Xie, M. Wilt, J. A. Willoughby and O. J. Rojas, *ACS Sustainable Chem. Eng.*, **6**, 1988 (2018).
28. P. Liu, N. Zhang, Y. Yi, M. E. Gibril, S. Wang and F. Kong, *Int. J. Biol. Macromol.*, **164**, 2312 (2020).
29. J. Bae, S. J. Park, O. S. Kwon and J. Jang, *Chem. Commun.*, **49**, 5456 (2013).
30. M. Zhao, J. Wang, C. Chong, X. Yu, L. Wang and Z. Shi, *RSC Adv.*, **5**, 101115 (2015).
31. K. Xia, Q. Ouyang, Y. Chen, X. Wang, X. Qian and L. Wang, *ACS Sustainable Chem. Eng.*, **4**, 159 (2016).
32. X. Dong, C. Lu, P. Zhou, S. Zhang, L. Wang and D. Lia, *RSC Adv.*, **5**, 42259 (2015).
33. D. I. Choi, J.-N. Lee, J. Song, P.-H. Kang, J.-K. Park and Y. M. Lee, *J. Solid State Electrochem.*, **17**, 2471 (2013).
34. A. Chithra, R. Rajeev and K. Prabhakaran, *Carbon Lett.*, **32**, 639 (2022).
35. N. Zhao, C. Wang, B. Li, W. Shen, F. Kang and Z.-H. Huang, *J. Mater. Sci.*, **57**, 11809 (2022).
36. D. Xuan, J. Liu, D. Wang, Z. Lu, Q. Liu, Y. Liu, S. Li and Z. Zheng, *Energy Fuels*, **35**, 796 (2021).
37. J. Bae, S. J. Park, O. S. Kwon and J. Jang, *J. Mater. Sci.*, **49**, 4323 (2014).
38. Y. S. Ho, D. J. Wase and C. Forster, *Environ. Technol.*, **17**, 71 (1996).
39. G. Mckay, M. Bino and A. Altamemi, *Water Res.*, **19**, 491 (1985).